

Decoding Long-duration Gravitational Waves from Binary Neutron Stars with Machine Learning: Parameter Estimation and Equations of State

Qian Hu,^{1,*} Jessica Irwin,¹ Qi Sun,² Christopher Messenger,¹ Lami Suleiman,³ Ik Siong Heng,¹ and John Veitch^{1,†}

¹*Institute for Gravitational Research, School of Physics and Astronomy,
University of Glasgow, Glasgow, G12 8QQ, United Kingdom*

²*Department of Computer Science, City University of Hong Kong, Tat Chee Avenue, Kowloon, Hong Kong SAR*

³*Nicholas and Lee Begovich Center for Gravitational Wave Physics and Astronomy,
California State University Fullerton, Fullerton, California 92831, USA*

(Dated: December 5, 2024)

Gravitational waves (GWs) from binary neutron stars (BNSs) offer valuable understanding of the nature of compact objects and hadronic matter. However, their analysis requires substantial computational resources due to the challenges in Bayesian stochastic sampling. The third-generation (3G) GW detectors are expected to detect BNS signals with significantly increased signal duration, detection rates, and signal strength, leading to a major computational burden in the 3G era. We demonstrate a machine learning-based workflow capable of producing source parameter estimation and constraints on equations of state (EOSs) for hours-long BNS signals in seconds with minimal hardware costs. We employ efficient compressions on the GW data and EOS using neural networks, based on which we build normalizing flows for inferences. Given that full Bayesian analysis is prohibitively time-intensive, we validate our model against (semi-)analytical predictions. Additionally, we estimate the computational demands of BNS signal analysis in the 3G era, showing that the machine learning methods will be crucial for future catalog-level analysis.

Introduction— The detection of gravitational waves (GWs) from binary neutron stars (BNSs) [1–3] has brought valuable insights into numerous problems in fundamental physics and astrophysics [2, 4–17]. In particular, neutron stars (NSs) experience deformation due to the strong tidal forces during the late stages of binary inspiral, revealing properties of hadronic matter in their extremely dense cores which have not been probed by any other experiments or observations. This makes BNS systems ideal probes of the equation of state (EOS) of NSs, shedding light on strong nuclear interactions in extreme conditions [4, 6, 8, 9, 13, 15–17]. Proposed third-generation (3G) GW detectors, including Einstein Telescope [18] and Cosmic Explorer [19], are expected to detect over 2×10^5 BNS events per year with enhanced signal-to-noise ratios (SNRs) [20, 21], offering remarkable potential for groundbreaking discoveries in fundamental particle physics.

However, a series of computationally intensive analyses are required for this purpose. After a BNS is detected, its source parameters, including component masses $m_{1,2}$ and tidal deformability parameters $\Lambda_{1,2}$, must be estimated from GW data [4, 17]. For current detectors, this is achieved through stochastic sampling under the Bayesian inference framework [22], which is the main bottleneck in data analysis due to its high time and hardware costs. With $\lesssim 10$ CPUs, it could take up to hours to days to analyze short-duration (< 32 s), low SNR (< 50) signals in current detectors. Moreover, the time cost of parameter estimation (PE) scales up with both SNR and signal duration. BNS signals in the 3G detectors may persist for hours due to the improved low-frequency sensitivity, rendering PE exceptionally slow. Although a number

of acceleration methods have been proposed, including reducing the size of the data [23, 24], speeding up the likelihood evaluation [25–30], and developing more efficient samplers [31, 32], limited progress has been made toward full PE for such signals in 3G detectors. Smith *et al.* [33] demonstrated the feasibility of using reduced-order-quadrature [25–27] to analyze long BNS signals and achieved 1600 CPU hours inference time. However, their experiment does not account for the Earth’s rotation, which is important for localizing long signals [34, 35] and adds additional computational demands to likelihood evaluations. Wong *et al.* [36] employed relative binning (also known as heterodyned likelihood) [28–30] and a gradient-based sampler, achieving 9600 CPU hours inference time for BNS events with potential GPU acceleration, however their example pertains to current detectors and assumes aligned-spin of the BNS system.

The subsequent inference of the EOS, which depends on the source PE, also requires Bayesian stochastic sampling [8]. The EOS describes the relationship between pressure (P) and density (ρ) of NS matter, which can be parameterized by piecewise polytropic [37] or spectral [38] representations. Posterior samples from PE can be used to infer parameters of these EOS representations, leading to the constraints of the P – ρ relation and reflecting the fundamental properties of hadronic interactions. The EOS inference alone can take tens to hundreds CPU hours per event, bringing further burden for the 3G catalogs.

Optimistically assuming 1000 CPU hours to process each event (PE+EOS) and 150 W CPU power, processing a catalog of 2×10^5 BNS events would consume 200 million CPU hours, 30 GWh of electricity and 4.8 mil-

lion USD in electricity charges per analysis run. This is a substantial burden on current international computing clusters, considering that the LIGO-Virgo-KAGRA (LVK) Computing Infrastructure [39] has fewer than 50k CPU cores - not to mention the budget constraints and environmental impacts. A more detailed estimation of computational costs for 3G detectors can be found in Ref. [40], where the authors obtain similar magnitudes.

Machine learning methods have shown considerable potential in efficient GW data analysis, including signal detection [41–43], parameter estimation [44–46] and subsequent astrophysical analyses [47–49]. Specifically, conditional normalizing flows (CNFs) [50, 51] are widely used as density estimators to approximate the true posterior distribution, which is traditionally obtained by Bayesian sampling. A CNF is a type of neural network that learns conditional differentiable and invertible transformations to convert the target posterior distribution to a simpler latent distribution (e.g. a multivariate Gaussian), dependent on observed data. It can take observational data as condition, and use it as part of the inputs to predict a conditional mapping between the latent and target distributions. During inference, samples can be rapidly drawn from the latent distribution and mapped back to the target posterior given a condition. A series of its successful applications in GW parameter estimation and subsequent probes into fundamental physics, primarily focusing on current detectors or short duration signals, can be found in Refs. [45, 52–55]. Notably, Dax *et al.* [55], applies CNFs to BNS signals, which is made possible using heterodyning and multibanding, along with a prior conditioning algorithm to train networks adaptable to different mass priors. We adopt a similar framework, but focus on longer signals and higher SNRs which represent the most challenging case in 3G detectors.

In this work, we develop a CNF-based analysis pipeline capable of generating full parameter estimation (with GW phase marginalized) for long signals from precessing BNSs in the 3G GW detectors, and generating EOS estimation within a second on a single GPU. The structure of the pipeline is shown in Fig. 1. The first CNF is conditioned on the preprocessed and compressed GW strain data to generate source PE, and the second CNF uses the PE results to infer the NS EOS. Details are provided below.

Parameter space (prior)— BNS parameters, especially the chirp mass, can be tightly constrained by 3G detectors [20, 21]. We find it is extremely challenging to train a model to cover a wide range of chirp mass and SNR, as the posterior is much narrower than the prior (training parameter space). To address this, we divide the parameter space to several regions and train a parameter estimation model for each. As an example, we consider two SNR ranges, 20-50 (low SNR) and 200-500 (high SNR). The former includes the majority of relatively informative BNS events in the 3G era, while the latter repre-

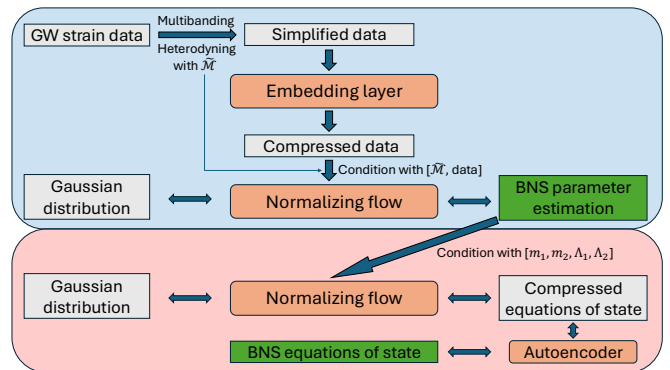


FIG. 1. Structure of our flow-based BNS analysis pipeline. The normalizing flows learn transforms between a Gaussian distribution and the target posterior distribution. The first flow is conditioned on the preprocessed (via multibanding and heterodyning) and compressed (by a neural network) GW strain data and generate source parameter estimation, which then conditions the second flow to generate a reduced representation of NS EOS. The reduced representation and original EOS can be transformed into each other by an neural autoencoder.

sents the louder ones. The detector frame chirp mass is sampled uniformly between $2 M_{\odot}$ and $2.1 M_{\odot}$ for low SNR prior, and $1.3 M_{\odot}$ and $1.31 M_{\odot}$ for high SNR prior. Given our detector configuration - one triangular ET at ET-D sensitivity [56] at the existing Virgo site and two 40-km CEs at CE2 design sensitivity [19] at Hanford and Livingston [57] - these mass and SNR ranges correspond to source-frame chirp masses consistent with current knowledge of BNS systems. The redshifts of low-SNR and high-SNR BNSs are ~ 0.1 and ~ 0.8 , respectively. The mass ratio $q = m_2/m_1$ is sampled uniformly between 0.5 and 1. The dimensionless spins are isotropic with the maximum magnitude of 0.05. Tidal deformability parameters are parameterized as $\tilde{\Lambda}$ and $\delta\tilde{\Lambda}$ [58], where $\tilde{\Lambda}$ is uniform between 0 and 1600 following the estimates from GW170817 [2], and $\delta\tilde{\Lambda}$ is uniform within its allowed range, which is determined by component masses and $\tilde{\Lambda}$ such that both components have positive deformability parameters. A wider prior for tidal parameters would benefit the applicability of our model in low mass scenarios, but here we start with 1600 as a proof-of-concept. The prior for extrinsic parameters follows common choices except for luminosity distance d_L : We sample the SNR uniformly in the target SNR band, then scale the d_L accordingly. This ensures the models consistently encounter similar loudness levels, reducing the number of outliers that are difficult to learn. Although our prior distribution is not perfectly aligned with those used in traditional parameter estimation, this data-independent discrepancy can be removed by importance sampling [53, 59].

Data preprocessing and compression— Considering a frequency band starting from 5 Hz, a three-hour-long

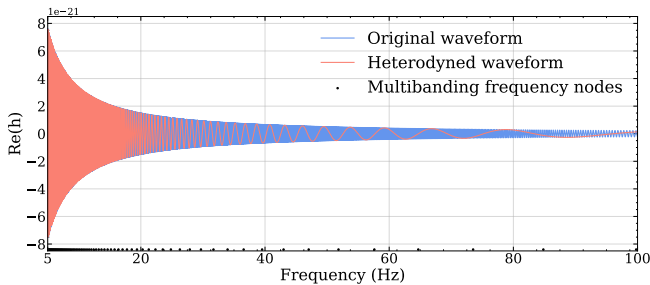


FIG. 2. BNS frequency-domain waveforms before (blue) and after (orange) heterodyning. Waveforms are truncated at 100 Hz for better illustration. Black dots represent the frequency nodes of the multibanding scheme, which bands defined between nodes.

BNS signal ($\sim 1.1 + 1.1 M_{\odot}$) with sampling rate of 2048 Hz has roughly 12 million data points, far too many to be used in traditional sampling algorithms. As the GW frequency increases during inspiral, a multibanding scheme [23, 24], i.e. adaptively adjusting the sampling frequency, is an effective way of reducing the data size and accelerating analyses. We propose a novel multibanding scheme that adaptively selects frequency nodes and resolutions, ensuring that each band’s resolution is precisely tuned to the needs of BNS signals. In particular, we divide the full bandwidth into bands containing roughly $N = 64$ data points each, and search from the high frequency cut-off f_0 (1024 Hz for this work) to lower frequencies until the first frequency f_1 such that

$$\alpha_{\text{safety}}(f_0 - f_1) [\tau(f_1) - \tau(f_0)] > N, \quad (1)$$

where $\tau(f)$ is the time-to-merger function to 3.5 post-Newtonian order [60], and $\alpha_{\text{safety}} = 2$ is a safety factor that enlarges the effective band duration, ensuring that the frequency resolution is high enough to cope with different source parameters and the potential errors in $\tau(f)$. The frequency resolution in the band (f_1, f_0) is given by

$$\Delta f_0 = \frac{1}{\alpha_{\text{safety}} [\tau(f_1) - \tau(f_0)]}, \quad (2)$$

which corresponds to $T_0 = \alpha_{\text{safety}} [\tau(f_1) - \tau(f_0)]$ data in the time domain. This process is repeated to obtain f_2, f_3, \dots and the corresponding Δf_i , until the lower frequency bound reaches the 5 Hz cut-off. This scheme reduces the 12 million data points to approximately 6000 in 81 bands. The selected frequency nodes are shown as black dots in fig. 2.

Singular Value Decomposition (SVD) is used to further compress the data by projecting it onto linear bases that represent the waveform space. However, a BNS waveform is highly oscillatory in the frequency domain, making SVD inefficient. Following Dax *et al.* [55], we employ heterodyning (relative binning) [28–30] to reduce the oscillation in the data (Fig. 2). Specifically, we multiply the signal by a phase factor $e^{i \frac{3}{128} (\frac{\pi G M f}{c^3})^{-5/3}}$, which

is the inverse of the leading term of the oscillations in GW waveform. This effectively smooths the waveform and improves the compression rate of SVD. With our restricted prior, we can retain the first 128 SVD bases sorted by singular values and reconstruct the zero-noise signal with a median mismatch of $\sim 10^{-8}$ and maximum mismatch of $\sim 10^{-6}$.

Neural networks are then used to further compress the SVD projection of data from multiple detectors. For cross-validation, we explore two types of neural networks for embedding: a residual network [61] of Multi-Layer Perceptrons (MLPResNet) and a Vision Transformer (ViT) [62]. However, due to the larger memory requirement of ViT, we only perform the cross-validation in low-SNR models. The five data streams from the 1ET+2CE network are compressed into a vector of length of 128, which is used to condition CNF for parameter estimation.

Training the parameter estimation model— The training set should comprehensively cover the parameter space, which, in analogy to template bank generation [63–66], becomes more challenging in low mass, high SNR and high dimension scenarios. Meeting all these factors, we find that large amount of training data is necessary to avoid overfitting.

GW strain data (signal and random Gaussian noise) is simulated on-the-fly during training using the waveform model IMRPhenomPv2_NRTidal [67]. Sky location parameters, coalescence time and SNR are randomly generated for each simulation, ensuring an infinite number of possible samples. The remaining 12 parameters are drawn from the prior before training and are used to calculate GW waveform. We save the SVD projections of the waveforms for loading during training. A total of 64 million samples are used to train low-SNR models, and 100 million samples are used for high-SNR models. Waveforms are projected to the detectors with the Earth’s rotation effects included. The CNF model used for PE is a neural spline flow [68]. Each PE model (embedding network and a CNF) has roughly 160 million learnable parameters with 96 million belonging to the normalizing flow, and all parameters optimized jointly by minimizing the negative log-likelihood. We train the networks for 2-3 weeks on an NVIDIA A100 GPU. Further technical details are given in Hu [69].

The chirp mass used for heterodyning is assumed to be perfectly known when obtaining SVD bases, but it is not known in inference. Following Dax *et al.* [55], during training, the GW data is heterodyned with $\tilde{\mathcal{M}} = \mathcal{M} + \delta\mathcal{M}$ instead of the exact chirp mass \mathcal{M} , where small perturbation $\delta\mathcal{M}$ enables the network to deal with inaccuracies in heterodyning. We set $\delta\mathcal{M}$ uniformly distributed in $[-0.0005, 0.0005] M_{\odot}$ for low-SNR models and $[-0.0001, 0.0001] M_{\odot}$ for high-SNR models. $\tilde{\mathcal{M}}$ is also given as a condition to the normalizing flow. During inference, the entire chirp mass prior can be divided into

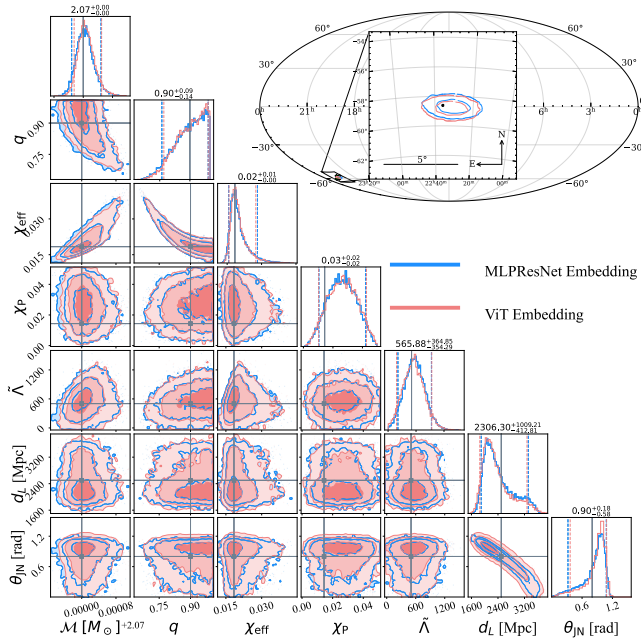


FIG. 3. Example corner plots and skymaps for low-SNR models. The blue region shows the posterior distribution generated by MLPResNet embedded model and the red is from ViT model. The source is a $1.74 + 1.56 M_{\odot}$ BNS system located at 2500 Mpc with a network SNR of 35. Dashed lines in corner plots show the 5% and 95% percentiles, and contours in skymaps are 50% and 90% confidence regions. The chirp mass is presented in the detector frame. The data is heterodyned with $\delta\mathcal{M} = 0.00014 M_{\odot}$.

several segments of length 0.001 (or 0.0002) M_{\odot} , with the segment yielding the highest likelihood being selected.

Parameter estimation results— We infer 16 out of the total 17 BNS parameters, with the coalescence phase marginalized by excluding it from the normalizing flow while still incorporating its underlying variations in the data. Example posteriors from low-SNR models are given in Fig. 3. Each posterior consists of 5000 samples drawn within ~ 0.25 s on an NVIDIA 3080Ti GPU. The models provide precise estimation of source parameters and correctly capture some parameter degeneracies, such as those between mass ratio q and effective spin χ_{eff} . As a cross-check, the two low-SNR models demonstrate good agreement.

Ideally, PE should be examined with several full PE runs using stochastic sampling. However, full PE of precessing BNS sources for the 3G detector network with the Earth rotation included had been a largely under-explored domain. Therefore, instead of meticulous comparison of posterior distributions, we assess the correctness of our PE models based on two criteria: precision and accuracy.

The precision, i.e., how tight the source parameters should be constrained, is examined with Fisher matrix formalism [70] and a semi-analytical Bayesian lo-

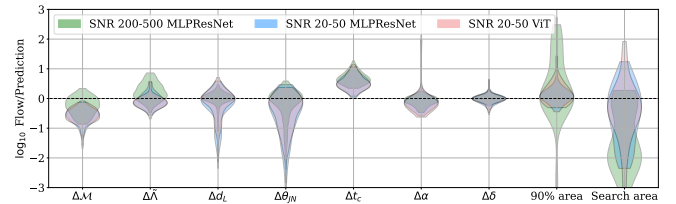


FIG. 4. Comparing PE from flow models with Fisher matrix and *SealGW*. The first seven columns display the ratios of the statistical uncertainties in the posterior distributions provided by the flow models relative to the Fisher matrix predictions. We show the results of chirp mass \mathcal{M} , tidal parameter $\tilde{\Lambda}$, luminosity distance d_L , inclination θ_{JN} , coalescence time t_c , right ascension α and declination δ . The last two columns compare the skymaps from the flow models with those from *SealGW*, showing the ratios of the 90% confidence area and searched area. Different models are represented by different colors. A black dashed line indicates where the flow models' results match those of the Fisher matrix or *SealGW*.

calization algorithm *SealGW* [35, 71]. The Fisher matrix formalism predicts the PE precision under high-SNR and Gaussian approximation, while *SealGW* gives better source localization as the sky parameter distributions are often non-Gaussian. However, we find the Fisher matrix is not perfectly reliable for the 17-dimensional problem as it predicts uncertainties of some parameters greater than their physical ranges. This is a common problem with the Fisher matrix formalism [20, 72]. However, it can still serve as a useful diagnostic tool that provides a sense of the PE precision.

Selecting the parameters for which the Fisher matrix gives reasonable results, the comparison is shown in Fig. 4. For most parameters, the ratio of statistical uncertainties peaks at 1, indicating agreement between the flow models and analytical predictions. Low-SNR flow models yield more precise estimations on chirp mass than the Fisher matrix, likely due to the inaccuracies in Fisher matrix in low-SNR, high dimensional scenarios, which improve in the high-SNR case. All flow models give broader constraints on coalescence time than the Fisher matrix. We observe that the CNF posteriors reveal a correlation between the tidal parameter $\tilde{\Lambda}$ and coalescence time t_c , which Fisher matrix does not capture. This correlation, arising from the effect of tidal deformation on the final stage of coalescence can be reproduced by reducing the Fisher matrix dimensionality, though at the expense of underestimating statistical uncertainties. Therefore, we conclude that the Fisher matrix could be inaccurate on coalescence time, but we can not rule out the possibility of the model not being optimally tuned. We also note that the Fisher matrix is evaluated at the injection parameters instead of the maximum likelihood parameters, which introduces a theoretical bias in the Fisher matrix estimates and broadens the spread of the uncertainty ratio.

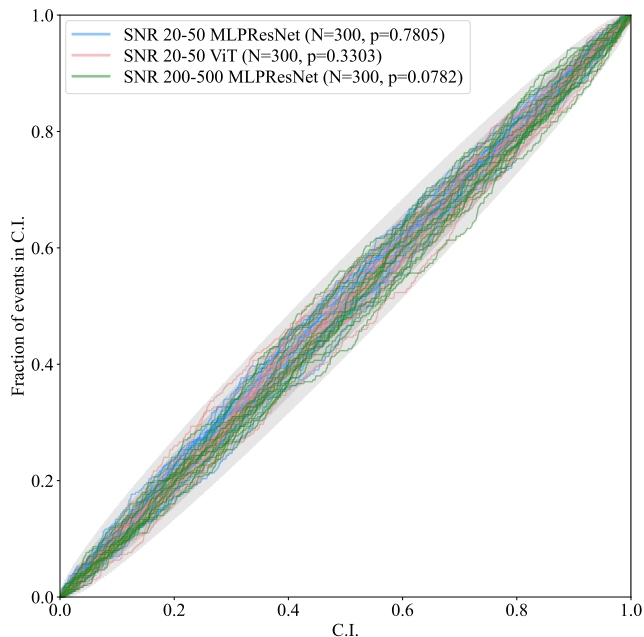


FIG. 5. P-P plots of prior all PE models. x -axis is the credible interval and y -axis the fraction of events included in the corresponding credible interval. Grey confidence regions are of 68%, 95%, 99.7% confidence levels. Different models are represented by different colors, while parameters for each model are plotted with the same color. p -values of different parameters are combined and are shown in the legend. $p < 0.05$ marks the failure of the p-p test.

Our flow models are able to provide precise localization of BNS sources with sky area mostly consistent with `SealGW`. The last column in fig. 4 compares the searched area, which measures the accuracy of source localization. The flow models outperform `SealGW` in localization accuracy especially in high SNR scenarios, likely due to approximations used in `SealGW`.

A more direct evaluation of PE accuracy is the p-p test which examines the self-consistency [73], in the sense that $x\%$ confidence interval should successfully predict $x\%$ of events. The p-p plots are shown in Fig. 5. All models pass the p-p test.

Constraining equations of state— Following McGinn *et al.* [47], we train another CNF based on RealNVP [74] to infer the NS EOS. The EOS used for training is generated using the publicly available code CUTER [75], which uses a semi-agnostic approach with a meta-model constrained by nuclear theory at low density, and piecewise polytropes at high density. We generate physically plausible BNS source parameters $\{m_1, m_2, \Lambda_1, \Lambda_2\}$ from each EOS. The CNF, conditioned on the BNS source parameters, is trained to infer a 12 dimensional representation of the EOS compressed by a convolutional auto-encoder, along with hyperparameters of each EOS, including maximum allowed pressure and energy density. The trained

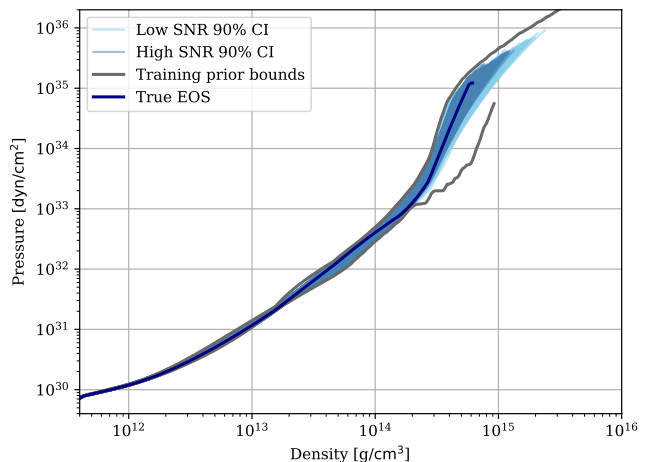


FIG. 6. 90% confidence intervals (CIs) of EOS constraints for simulated BNS events. The CIs are defined in the 12D representation space and mapped to pressure-density plane by the auto-encoder. Two BNS events, governed by the same EOS, have different network SNRs: 39 (low-SNR, in light blue) and 390 (high-SNR, in blue). The injected EOS is given in dark blue with the training prior bounds given in grey, illustrating the most stiff and most soft EOSs in our training data set.

auto-encoder can then reconstruct the $P - \rho$ EOS by providing the 12 dimensional representation.

We simulate two BNS events with identical underlying EOS but differing network SNRs of 39 and 390 and then perform parameter estimation with our PE models. The resulting posterior samples are passed to the EOS inference model to generate EOS posteriors (samples of 12D representation plus hyperparameters), which are then decoded into pressure-density relationships using the auto-encoder (Fig. 6). We successfully recover the underlying EOS in both cases, with tighter constraints in the high-SNR scenario as expected. The EOS inference takes less than one second, greatly reducing the computation cost compared with traditional stochastic sampling.

Discussions— We demonstrate a reliable machine learning based analysis pipeline for long BNS signals in the 3G GW detectors. While certain tasks could be prohibitively slow for traditional methods, our approach processes each event in under a second on a single GPU. This efficiency is crucial for enabling catalog-level analyses in the 3G era. Assuming one second sampling time and one minutes pre- and post- processing CPU time for PE+EOS analysis per event, the energy cost for analyzing the catalog mentioned in the introduction reduces to 508 kWh, costing approximately 81 USD. For the training cost, assuming 500 models to cover the parameter space, and each requiring two weeks of training, the training would cost 25.2 MWh and 4000 USD, totaling 25.7 MWh and 4100 USD together with inference. This is more than a thousand times less than traditional methods. Our

model, therefore, presents a feasible and exciting opportunity to advance population-level knowledge of hadronic matter and NS, along with other follow-up science such as cosmology [12, 76, 77], astrophysical population [78–80], stochastic background [81–83], etc. We also note that the 500 models could be an overestimation according to Ref. [55], in which the authors have shown that the CNF framework can be trained on a wider prior, which further reduces the computational costs.

Several potential improvements could enhance our models further. For example, instead of randomly drawing parameters to build training sets of PE models, we could find a more efficient training set that has a smaller size and reduces the training cost. Additionally, importance sampling could be used to improve the accuracy of PE. For EOS inference, combining multiple events would significantly tighten the EOS constraints, as the true underlying EOS would pass posterior parameter regions of all BNS events. Intuitively, this is a more effective way to improve EOS constraints than improving the SNR, because a single tight posterior region still allows a certain level of flexibility in EOS. We also note that the EOS could be constrained better with a higher frequency cut-off in PE.

Looking ahead, there is also a pressing need to adapt these algorithms to more realistic scenarios expected in the 3G detectors. This includes addressing challenges including time variations in noise, overlapping signals, etc [84–89], ensuring that the analysis methods remain robust and reliable under all conditions. These improvements and challenges will be explored in our future work.

Acknowledgments— The authors would like to thank Nihar Gupte, Maximilian Dax, Xue-Ting Zhang, and Michael Puerrer for helpful discussions and suggestions. The authors are grateful for computational resources provided by the LIGO Lab at Caltech which is supported by National Science Foundation Grants PHY-0757058 and PHY-0823459. QH is supported by STFC grant ST/Y004256/1 and CSC. JV is supported by STFC grant ST/Y004256/1.

* Qian.Hu@glasgow.ac.uk

† John.Veitch@glasgow.ac.uk

- [1] B. P. Abbott *et al.*, *Physical Review Letters* **119**, 30 (2017).
- [2] B. P. Abbott *et al.*, *Physical Review X* **9**, 11001 (2019).
- [3] B. P. Abbott *et al.*, *The Astrophysical Journal* **848**, L12 (2017).
- [4] S. De, D. Finstad, J. M. Lattimer, D. A. Brown, E. Berger, and C. M. Biwer, *Phys. Rev. Lett.* **121**, 091102 (2018), [Erratum: *Phys.Rev.Lett.* 121, 259902 (2018)], [arXiv:1804.08583 \[astro-ph.HE\]](#).
- [5] K. P. Mooley, A. T. Deller, O. Gottlieb, E. Nakar, G. Hallinan, S. Bourke, D. A. Frail, A. Horesh, A. Corsi, and K. Hotokezaka, *Nature* **561**, 355 (2018), [arXiv:1806.09693 \[astro-ph.HE\]](#).
- [6] C. D. Capano, I. Tews, S. M. Brown, B. Margalit, S. De, S. Kumar, D. A. Brown, B. Krishnan, and S. Reddy, *Nature Astron.* **4**, 625 (2020), [arXiv:1908.10352 \[astro-ph.HE\]](#).
- [7] M. Nicholl *et al.*, *Astrophys. J. Lett.* **848**, L18 (2017), [arXiv:1710.05456 \[astro-ph.HE\]](#).
- [8] B. P. Abbott *et al.* (LIGO Scientific, Virgo), *Phys. Rev. Lett.* **121**, 161101 (2018), [arXiv:1805.11581 \[gr-qc\]](#).
- [9] E. Annala, T. Gorda, A. Kurkela, and A. Vuorinen, *Phys. Rev. Lett.* **120**, 172703 (2018), [arXiv:1711.02644 \[astro-ph.HE\]](#).
- [10] D. Kasen, B. Metzger, J. Barnes, E. Quataert, and E. Ramirez-Ruiz, *Nature* **551**, 80 (2017), [arXiv:1710.05463 \[astro-ph.HE\]](#).
- [11] B. Margalit and B. D. Metzger, *Astrophys. J. Lett.* **850**, L19 (2017), [arXiv:1710.05938 \[astro-ph.HE\]](#).
- [12] B. P. Abbott *et al.* (LIGO Scientific, Virgo, 1M2H, Dark Energy Camera GW-E, DES, DLT40, Las Cumbres Observatory, VINROUGE, MASTER), *Nature* **551**, 85 (2017), [arXiv:1710.05835 \[astro-ph.CO\]](#).
- [13] G. Baym, T. Hatsuda, T. Kojo, P. D. Powell, Y. Song, and T. Takatsuka, *Rept. Prog. Phys.* **81**, 056902 (2018), [arXiv:1707.04966 \[astro-ph.HE\]](#).
- [14] M. M. Kasliwal *et al.*, *Science* **358**, 1559 (2017), [arXiv:1710.05436 \[astro-ph.HE\]](#).
- [15] E. Annala, T. Gorda, A. Kurkela, J. Nättilä, and A. Vuorinen, *Nature Phys.* **16**, 907 (2020), [arXiv:1903.09121 \[astro-ph.HE\]](#).
- [16] A. Bauswein, N.-U. F. Bastian, D. B. Blaschke, K. Chatziioannou, J. A. Clark, T. Fischer, and M. Oertel, *Phys. Rev. Lett.* **122**, 061102 (2019), [arXiv:1809.01116 \[astro-ph.HE\]](#).
- [17] T. Dietrich, M. W. Coughlin, P. T. H. Pang, M. Bulla, J. Heinzel, L. Issa, I. Tews, and S. Antier, *Science* **370**, 1450 (2020), [arXiv:2002.11355 \[astro-ph.HE\]](#).
- [18] M. Punturo *et al.*, *Class. Quant. Grav.* **27**, 194002 (2010).
- [19] D. Reitze and et al, “Cosmic Explorer: The U.S. Contribution to Gravitational-Wave Astronomy beyond LIGO,” (2019), [arXiv:1907.04833 \[astro-ph, physics:gr-qc\]](#).
- [20] S. Borhanian and B. S. Sathyaprakash, “Listening to the Universe with Next Generation Ground-Based Gravitational-Wave Detectors,” (2022), [arXiv:2202.11048 \[gr-qc\]](#).
- [21] M. Branchesi *et al.*, *JCAP* **07**, 068 (2023), [arXiv:2303.15923 \[gr-qc\]](#).
- [22] J. Veitch *et al.*, *Phys. Rev. D* **91**, 042003 (2015), [arXiv:1409.7215 \[gr-qc\]](#).
- [23] S. Vinciguerra, J. Veitch, and I. Mandel, *Class. Quant. Grav.* **34**, 115006 (2017), [arXiv:1703.02062 \[gr-qc\]](#).
- [24] S. Morisaki, *Phys. Rev. D* **104**, 044062 (2021), [arXiv:2104.07813 \[gr-qc\]](#).
- [25] P. Canizares, S. E. Field, J. R. Gair, and M. Tiglio, *Phys. Rev. D* **87**, 124005 (2013), [arXiv:1304.0462 \[gr-qc\]](#).
- [26] P. Canizares, S. E. Field, J. Gair, V. Raymond, R. Smith, and M. Tiglio, *Phys. Rev. Lett.* **114**, 071104 (2015), [arXiv:1404.6284 \[gr-qc\]](#).
- [27] R. Smith, S. E. Field, K. Blackburn, C.-J. Haster, M. Pürrer, V. Raymond, and P. Schmidt, *Phys. Rev. D* **94**, 044031 (2016), [arXiv:1604.08253 \[gr-qc\]](#).
- [28] N. J. Cornish, “Fast Fisher Matrices and Lazy Likelihoods,” (2010), [arXiv:1007.4820 \[gr-qc\]](#).
- [29] B. Zackay, L. Dai, and T. Venumadhav, “Relative Bin-

- ning and Fast Likelihood Evaluation for Gravitational Wave Parameter Estimation,” (2018), arXiv:1806.08792 [astro-ph.IM].
- [30] N. Leslie, L. Dai, and G. Pratten, *Phys. Rev. D* **104**, 123030 (2021), arXiv:2109.09872 [astro-ph.IM].
- [31] M. J. Williams, J. Veitch, and C. Messenger, *Phys. Rev. D* **103**, 103006 (2021), arXiv:2102.11056 [gr-qc].
- [32] K. W. K. Wong, M. Gabrié, and D. Foreman-Mackey, *The Journal of Open Source Software* **8**, 5021 (2023), arXiv:2211.06397 [astro-ph.IM].
- [33] R. Smith *et al.*, *Phys. Rev. Lett.* **127**, 081102 (2021), arXiv:2103.12274 [gr-qc].
- [34] W. Zhao and L. Wen, *Phys. Rev. D* **97**, 064031 (2018), arXiv:1710.05325 [astro-ph.CO].
- [35] Q. Hu and J. Veitch, *Astrophys. J. Lett.* **958**, L43 (2023), arXiv:2309.00970 [gr-qc].
- [36] K. W. K. Wong, M. Isi, and T. D. P. Edwards, *Astrophys. J.* **958**, 129 (2023), arXiv:2302.05333 [astro-ph.IM].
- [37] J. S. Read, B. D. Lackey, B. J. Owen, and J. L. Friedman, *Phys. Rev. D* **79**, 124032 (2009), arXiv:0812.2163 [astro-ph].
- [38] L. Lindblom, *Phys. Rev. D* **82**, 103011 (2010), arXiv:1009.0738 [astro-ph.HE].
- [39] S. Bagnasco, “The Ligo-Virgo-KAGRA Computing Infrastructure for Gravitational-wave Research,” (2023), arXiv:2311.12559 [astro-ph.IM].
- [40] Q. Hu and J. Veitch, (2024), arXiv:2412.02651 [gr-qc].
- [41] T. D. Gebhard, N. Kilbertus, I. Harry, and B. Schölkopf, *Phys. Rev. D* **100**, 063015 (2019), arXiv:1904.08693 [astro-ph.IM].
- [42] M. B. Schäfer *et al.*, *Phys. Rev. D* **107**, 023021 (2023), arXiv:2209.11146 [astro-ph.IM].
- [43] V. Skliris, M. R. K. Norman, and P. J. Sutton, (2020), 10.48550/arXiv.2009.14611, arXiv:2009.14611 [astro-ph.IM].
- [44] H. Gabbard, C. Messenger, I. S. Heng, F. Tonolini, and R. Murray-Smith, *Nature Phys.* **18**, 112 (2022), arXiv:1909.06296 [astro-ph.IM].
- [45] M. Dax, S. R. Green, J. Gair, J. H. Macke, A. Buonanno, and B. Schölkopf, *Phys. Rev. Lett.* **127**, 241103 (2021), arXiv:2106.12594 [gr-qc].
- [46] J. Langendorff, A. Kolmus, J. Janquart, and C. Van Den Broeck, *Phys. Rev. Lett.* **130**, 171402 (2023), arXiv:2211.15097 [gr-qc].
- [47] J. McGinn, A. Mukherjee, J. Irwin, C. Messenger, M. J. Williams, and I. S. Heng, “Rapid neutron star equation of state inference with Normalising Flows,” (2024), arXiv:2403.17462 [gr-qc].
- [48] F. Stachurski, C. Messenger, and M. Hendry, *Phys. Rev. D* **109**, 123547 (2024), arXiv:2310.13405 [gr-qc].
- [49] D. Ruhe, K. Wong, M. Cranmer, and P. Forré, “Normalizing Flows for Hierarchical Bayesian Analysis: A Gravitational Wave Population Study,” (2022), arXiv:2211.09008 [astro-ph.IM].
- [50] I. Kobyzev, S. J. Prince, and M. A. Brubaker, *IEEE transactions on pattern analysis and machine intelligence* **43**, 3964 (2020).
- [51] G. Papamakarios, E. Nalisnick, D. J. Rezende, S. Mohamed, and B. Lakshminarayanan, *Journal of Machine Learning Research* **22**, 1 (2021).
- [52] S. R. Green and J. Gair, *Mach. Learn. Sci. Tech.* **2**, 03LT01 (2021), arXiv:2008.03312 [astro-ph.IM].
- [53] M. Dax, S. R. Green, J. Gair, M. Pürrer, J. Wildberger, J. H. Macke, A. Buonanno, and B. Schölkopf, *Phys. Rev. Lett.* **130**, 171403 (2023), arXiv:2210.05686 [gr-qc].
- [54] N. Gupte *et al.*, “Evidence for eccentricity in the population of binary black holes observed by LIGO-Virgo-KAGRA,” (2024), arXiv:2404.14286 [gr-qc].
- [55] M. Dax, S. R. Green, J. Gair, N. Gupte, M. Pürrer, V. Raymond, J. Wildberger, J. H. Macke, A. Buonanno, and B. Schölkopf, “Real-time gravitational-wave inference for binary neutron stars using machine learning,” (2024), arXiv:2407.09602 [gr-qc].
- [56] S. Hild *et al.*, *Class. Quant. Grav.* **28**, 094013 (2011), arXiv:1012.0908 [gr-qc].
- [57] B. P. Abbott *et al.* (LIGO Scientific), *Class. Quant. Grav.* **34**, 044001 (2017), arXiv:1607.08697 [astro-ph.IM].
- [58] L. Wade, J. D. E. Creighton, E. Ochsner, B. D. Lackey, B. F. Farr, T. B. Littenberg, and V. Raymond, *Phys. Rev. D* **89**, 103012 (2014).
- [59] A. H. Nitz, “Robust, Rapid, and Simple Gravitational-wave Parameter Estimation,” (2024), arXiv:2410.05190 [astro-ph.IM].
- [60] A. Buonanno, B. Iyer, E. Ochsner, Y. Pan, and B. S. Sathyaprakash, *Phys. Rev. D* **80**, 084043 (2009), arXiv:0907.0700 [gr-qc].
- [61] K. He, X. Zhang, S. Ren, and J. Sun, (2015), 10.48550/arXiv.1512.03385, arXiv:1512.03385.
- [62] A. Dosovitskiy *et al.*, “An image is worth 16x16 words: Transformers for image recognition at scale,” (2021), arXiv:2010.11929 [cs.CV].
- [63] B. S. Sathyaprakash and S. V. Dhurandhar, *Phys. Rev. D* **44**, 3819 (1991).
- [64] D. A. Brown, I. Harry, A. Lundgren, and A. H. Nitz, *Phys. Rev. D* **86**, 084017 (2012), arXiv:1207.6406 [gr-qc].
- [65] I. Harry, S. Privitera, A. Bohé, and A. Buonanno, *Phys. Rev. D* **94**, 024012 (2016), arXiv:1603.02444 [gr-qc].
- [66] A. H. Nitz and Y.-F. Wang, *Phys. Rev. Lett.* **127**, 151101 (2021), arXiv:2106.08979 [astro-ph.HE].
- [67] T. Dietrich, A. Samajdar, S. Khan, N. K. Johnson-McDaniel, R. Dudi, and W. Tichy, *Phys. Rev. D* **100**, 044003 (2019), arXiv:1905.06011 [gr-qc].
- [68] C. Durkan, A. Bekasov, I. Murray, and G. Papamakarios, in *Advances in Neural Information Processing Systems*, Vol. 32, edited by H. Wallach, H. Larochelle, A. Beygelzimer, F. d’Alché-Buc, E. Fox, and R. Garnett (Curran Associates, Inc., 2019).
- [69] Q. Hu, *Towards high-precision gravitational wave astronomy: robust and efficient data analysis for ground-based detectors*, Ph.D. thesis, University of Glasgow (2024).
- [70] L. S. Finn, *Phys. Rev. D* **46**, 5236 (1992), arXiv:gr-qc/9209010.
- [71] Q. Hu, C. Zhou, J.-H. Peng, L. Wen, Q. Chu, and M. Kovalam, *Phys. Rev. D* **104**, 104008 (2021), arXiv:2110.01874 [gr-qc].
- [72] M. Vallisneri, *Phys. Rev. D* **77**, 042001 (2008), arXiv:gr-qc/0703086.
- [73] T. Sidery, B. Aylott, N. Christensen, B. Farr, W. Farr, F. Feroz, J. Gair, K. Grover, P. Graff, C. Hanna, V. Kalogera, I. Mandel, R. O’Shaughnessy, M. Pitkin, L. Price, V. Raymond, C. Röver, L. Singer, M. van der Sluys, R. J. E. Smith, A. Vecchio, J. Veitch, and S. Vitale, *Phys. Rev. D* **89**, 084060 (2014).
- [74] L. Dinh, J. Sohl-Dickstein, and S. Bengio, “Density estimation using real nvp,” (2017), arXiv:1605.08803 [cs.LG].
- [75] P. J. Davis, H. D. Thi, A. F. Fantina, F. Gulminelli, M. Oertel, and L. Suleiman, *Astron. Astrophys.* **687**,

- A44 (2024), arXiv:2406.14906 [astro-ph.HE].
- [76] M. Soares-Santos *et al.* (DES, LIGO Scientific, Virgo), *Astrophys. J. Lett.* **876**, L7 (2019), arXiv:1901.01540 [astro-ph.CO].
- [77] B. P. Abbott *et al.* (LIGO Scientific, Virgo, VIRGO), *Astrophys. J.* **909**, 218 (2021), arXiv:1908.06060 [astro-ph.CO].
- [78] B. P. Abbott *et al.* (LIGO Scientific, Virgo), *Astrophys. J. Lett.* **882**, L24 (2019), arXiv:1811.12940 [astro-ph.HE].
- [79] R. Abbott *et al.* (LIGO Scientific, Virgo), *Astrophys. J. Lett.* **913**, L7 (2021), arXiv:2010.14533 [astro-ph.HE].
- [80] R. Abbott *et al.* (KAGRA, VIRGO, LIGO Scientific), *Phys. Rev. X* **13**, 011048 (2023), arXiv:2111.03634 [astro-ph.HE].
- [81] B. P. Abbott *et al.* (LIGO Scientific, Virgo), *Phys. Rev. Lett.* **118**, 121101 (2017), [Erratum: Phys.Rev.Lett. 119, 029901 (2017)], arXiv:1612.02029 [gr-qc].
- [82] B. P. Abbott *et al.* (LIGO Scientific, Virgo), *Phys. Rev. Lett.* **118**, 121102 (2017), arXiv:1612.02030 [gr-qc].
- [83] B. P. Abbott *et al.* (LIGO Scientific, Virgo), *Phys. Rev. Lett.* **120**, 091101 (2018), arXiv:1710.05837 [gr-qc].
- [84] Y. Himemoto, A. Nishizawa, and A. Taruya, *Physical Review D* **104**, 044010 (2021), arxiv:2103.14816 [astro-ph, physics:gr-qc].
- [85] E. Pizzati, S. Sachdev, A. Gupta, and B. Sathyaprakash, *Physical Review D* **105**, 104016 (2022), arxiv:2102.07692 [astro-ph, physics:gr-qc].
- [86] P. Relton and V. Raymond, *Physical Review D* **104**, 084039 (2021), arxiv:2103.16225 [astro-ph, physics:gr-qc].
- [87] P. Relton, A. Virtuoso, S. Bini, V. Raymond, I. Harry, M. Drago, C. Lazzaro, A. Miani, and S. Tiwari, *Physical Review D* **106**, 104045 (2022), arxiv:2208.00261 [astro-ph, physics:gr-qc].
- [88] A. Samajdar, J. Janquart, C. V. D. Broeck, and T. Dietrich, *Physical Review D* **104**, 044003 (2021), arxiv:2102.07544 [astro-ph, physics:gr-qc].
- [89] Q. Hu and J. Veitch, *Astrophys. J.* **945**, 103 (2023), arXiv:2210.04769 [gr-qc].